Arab J Sci Eng (2016) 41:4867–4878
DOI 10.1007/s13369-016-2182-7

RESEARCH ARTICLE - CIVIL ENGINEERING

Areal Change Detection and 3D Modeling of Mine Lakes Using High-Resolution Unmanned Aerial Vehicle Images

Mehmet Ali Yucel[1] · **Recep Yavuz Turan**[2]

Received: 9 February 2016 / Accepted: 26 April 2016 / Published online: 18 May 2016

Abstract This study focuses on the Etili and Comakli open-pit coal mines, where mine lakes are most densely located within the Can Coal Basin (northwestern Turkey). The aim of our study was to create 3D terrain models of these mine lakes using high-resolution images from an unmanned aerial vehicle (UAV) and to quantify areal changes linked to anthropogenic and meteorological effects over the study period. In November 2014 and October 2015, a DJI F550 hexacopter was flown at elevations of 30–100 m, and images were acquired using a 12-megapixel camera. Nineteen flights were completed, with each flight acquiring between 109 and 554 images. 3D modeling of UAV images was carried out with Agisoft software, using the most common structure from motion algorithm. Its workflow, involving image matching, georeferencing, digital elevation modeling, orthomosaics, 3D point cloud, and 3D textured model creation, was used to generate our 3D terrain model for the mine lakes. Orthomosaics with 1–6 cm/pixel resolution were used to assess areal change in the mine lakes. Area was calculated using two different methods (digitization and classification) within the ArcGIS package; results of these two methods were compared. Our UAV study of open-pit mines rapidly and precisely determined changes in topography linked to anthropogenic and meteorological effects. It also proved to be an effective method of visualizing such effects over the short term.

✉ Mehmet Ali Yucel
aliyucel@comu.edu.tr

[1] Department of Geomatics Engineering, Canakkale Onsekiz Mart University, Canakkale, Turkey

[2] Department of Electronics and Automation, Canakkale Onsekiz Mart University, Canakkale, Turkey

Keywords Unmanned aerial vehicle (UAV) · Mine lakes · 3D Terrain modeling · Areal change detection

1 Introduction

Unmanned aerial vehicles (UAVs) are remotely piloted aircraft equipped with digital cameras that can be used to acquire a time series of high-resolution aerial images for mapping and monitoring of the environment. This method is low cost and has a flexible deployment [1–3]. UAV applications can be used to create an orthomosaic, a digital elevation model (DEM), as well as 3D point cloud and 3D terrain models. The scale, resolution, and precision of ground control points are the major factors affecting UAV image quality [4,5]. In recent years, UAV-based applications have been developed to provide convenient geotechnical and environmental monitoring solutions, illustrated by the following examples. Niethammer et al. [4] investigated the use of UAV for high-resolution measurements of landslides. Mancini et al. [6] used UAV systems for high-resolution reconstruction of topography in coastal environments. Immerzeel et al. [7] monitored Himalayan glacier dynamics using high-resolution UAV images and Agisoft software (Agisoft LLC, Russia). Siebert and Teizer [8] focused on mobile 3D mapping of earthwork projects using UAV systems. Martin et al. [9] used UAVs for mapping uranium mines. The accuracy of 3D surfaces reconstructed from UAV images was evaluated by Douterloigne et al. [10] and James and Robson [11], while Wang et al. [2] determined the accuracy of 3D geometry from low-attitude UAV images at the Zijin Mine in China. Fonstad et al. [12] tested the utility of the structure from motion (SfM) approach using UAV imagery in a bedrock fluvial setting.

In particular, the SfM algorithm defined by Lowe [13] matches images by finding the same details on image pairs

using a scale invariant feature transform algorithm. Koutsoudis et al. [14] reconstructed an Ottoman monument, Javernick et al. [15] modeled the topography of shallow braided rivers, Goncalves and Henriques [16] analyzed UAV mapping and monitoring of sand dunes and beaches, while Tavani et al. [17] created a 3D digital model of the Khaviz Anticline (Iran) from a set of non-oriented images, all using the Agisoft SfM workflow. Some of the other methods used in reconstruction of a 3D point cloud from image sequences are semi-global matching (SGM), MicMac (a photogrammetry software library developed by the French Geographical Institute), and a patch-based multiview stereo (PMVS) method. SGM is a stereo image-matching approach using a four-step method for dense image matching of image pairs [18,19]. MicMac supports matching point extraction with a scale invariant feature transform operator and generates a dense point cloud in a multiview approach [19,20]. PMVS acquires a dense model using the output of bundler and images [19,21,22]. The PMVS method generates a scaled point cloud, with better accuracy than SGM or MicMac. Thus, the SfM approach is the most useful and accurate method available to create 3D point cloud and 3D models using low-altitude aerial images collected by a UAV [23,24].

Anthropogenic landscapes cover a great deal of the Earth's surface [25,26], and in such landscapes, direct anthropogenic disturbances of surface morphology and processes are significant [27–29]. Coal mining activities can have a significant impact on the geomorphology and hydrology of catchments, both during mining and for many years after their cessation [29,30]. Open- pit coal mining has severe ecological effects, with alterations that affect vegetation, soil, bedrock, and landforms [31]. Acid mine drainage is an anthropogenic process caused by sulfide mineralization, occurring because of mining activity and grain-size reduction [32]. Acid mine lakes form from mine wastes having high acidity, typically caused by high concentrations of sulfate and toxic metals. They create an environmental threat through degradation and diminishing of surface water, groundwater, soil quality, and food quality, and may kill fish, flora, and most organisms in the local waters and soils [33–36].

In the Can Coal Basin, the Etili and Comakli mines have operated as open pits since the 1980s. During the production of coal with high sulfur content from the Can formation at these sites, the topography was degraded, forming large depressions. When mining activities ceased without any accompanying rehabilitation measures, these depressions filled with surface and ground waters. Many factors, involving both coal and volcanic rocks rich in pyrite, bacterial activity, meteorological factors, and lack of acid-neutralizing rocks, have contributed to acid mine drainage at the Etili site [37]. Since mining activities ceased, the rate of acid mine drainage has increased, with the increase in material with reduced grain size. A number of studies have addressed this process in this area. For example, Bozcu et al. [38] examined the Can Coal Basin geology, Gurdal and Bozcu [39] identified the petrographic characteristics of the coal, while Gunduz and Baba [40], Okumusoglu and Gunduz [41], Sanliyuksel Yucel and Baba [42], Sanliyuksel Yucel and Baba [43] studied the hydrogeochemical characteristics of the acid mine lakes. In addition, Sanliyuksel Yucel et al. [44] identified areal changes in these acid mine lakes using satellite images from different years, while Sanliyuksel Yucel et al. [37] established their formation processes. The aim of this study is to use high-resolution UAV images for the first time to model the mine lakes in three dimensions in the study area. These data also are used to evaluated changes to their lake areas over two consecutive years using both digitization and classification methods, as well as to identify anthropogenic and meteorological effects on these areal changes.

2 Description of the Study Area

The study area is geographically located in the Can Coal Basin in the Canakkale Province of northwestern Turkey (Fig. 1a). The Can Coal Basin, containing nearly 100 Mt of coal, is a NE–SW- oriented, 30–35 km long and 8–10 km wide depression [38]. Our study involved UAV imaging of nine different mine lakes in the Etili area, and four mine lakes in Comakli area of the Can Coal Basin (Fig. 1b–d). The lakes at the Etili site are referred to as E1–E9, while lakes at the Comakli site are referred to as C1–C4. All lakes at the Etili site, as well as C1 and C2 at Comakli are acidic, with pH values below 4. At the Comakli site, C3 and C4 have pH values above 7. The alkaline character of C3 and C4 is related to water draining local limestone blocks outcropping to the southeast of Comakli, which increases the pH value of these lakes. Mine lakes are situated within the elevation range of 128–245 m above mean sea level. They are located upstream of the Kocabas Stream, which passes through the Can District, before flowing into the Sea of Marmara. Along this stream, several residential areas supply their drinking water from boreholes. Thus, the water quality of the Kocabas Stream and its tributaries is critical to local residents. The hydrology of surface drainage in the Can Coal Basin has a variable flow regime, dependent upon precipitation patterns and temperature.

Gunduz and Baba [40] stated that C1 had a pH of 3.07 and contained high concentrations of SO_4, Al, Fe and Mn, with values of 3923, 109.92, 74.09 and 51.49 mg/l, respectively. Sanliyuksel Yucel and Baba [42] found that according to the water pollution control regulations in Turkey, the mine lakes in the Etili area had pH, SO_4, Al, Fe, Mn, Ni and Zn values in class IV, classifying them as very polluted waters. These regulations state that such lake waters should not be used

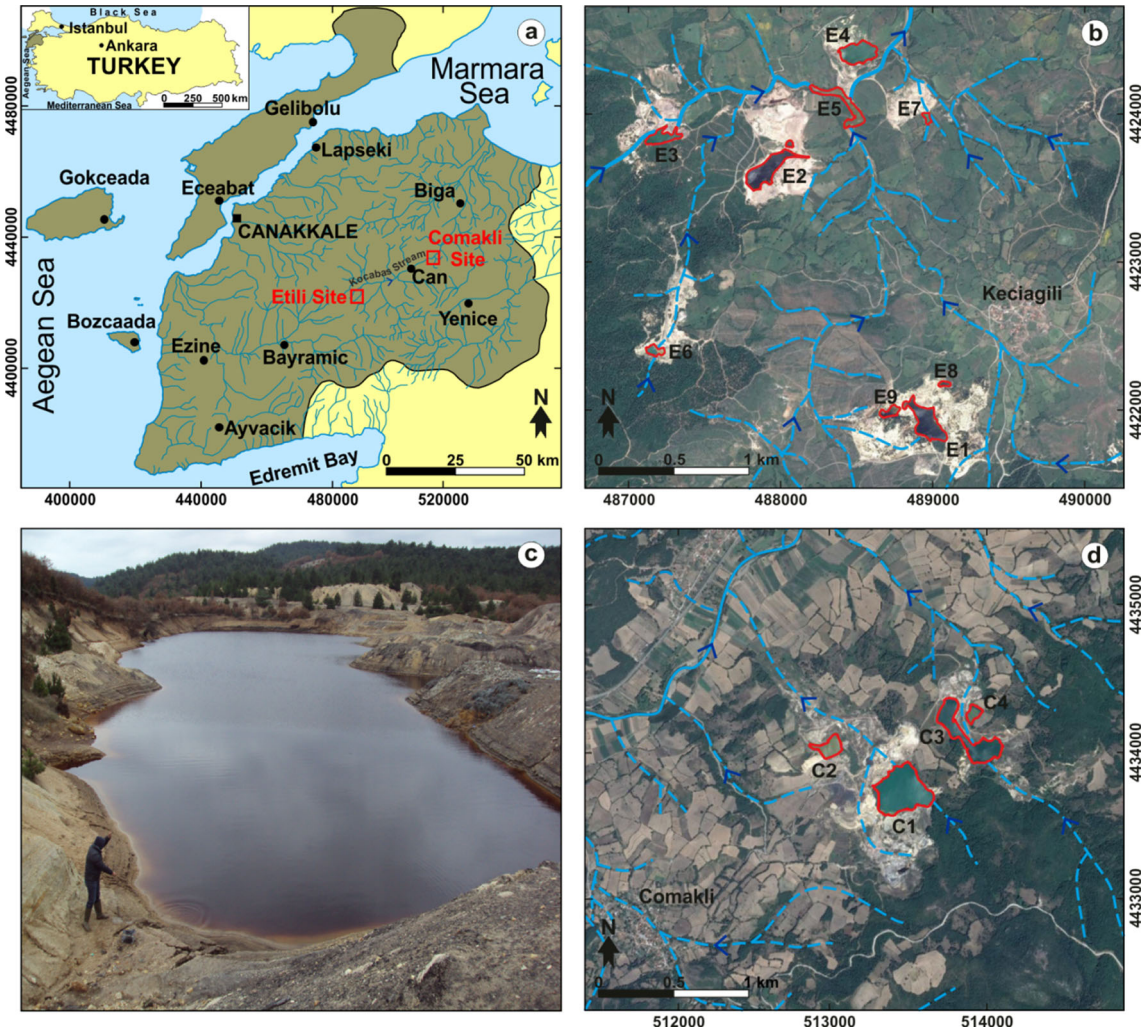

Fig. 1 **a** Location map of the study area. **b** Etili site on Pleiades satellite image, May 2013. **c** Snapshot from E2. **d** Comakli site on Pleiades satellite image, August 2013

for any reason. Sanliyuksel Yucel and Baba [43] stated that the creeks surrounding the mine lakes at Etili had pH values varying from 2.85 to 5.75, and their waters had a red-brown color. Typically, when mine operators reopen coal pits, they empty these acid mine lakes into local creeks; this occurred several times during our study. One of the important management points of acid mine drainage is that in addition to its soluble pollutants, it has harmful effects on environments in near, and even distant, surroundings related to its transport. Acidic drainage carried by surface waters comes into contact with different rocks and soils, and may even reach agricultural areas. It is also worth noting that in the Can Coal Basin, fish deaths have occurred because of seepage and discharge of acid mine lakes into local creeks [42,43,45]. Thus, contaminated surface drainage waters, with low pH and high metal concentrations, transported long distances by local streams, create a great risk in terms of environmental quality.

3 Experimental Methods

3.1 Global Navigation Satellite System (GNSS) Survey

As ground control points (GCPs), 50 × 70 cm^2 colored cardboard sheets were located throughout the study area before each flight. The number of GCPs used while capturing images varied from 6 to 15, depending on the size of the lake. The location of GCPs around E1 and E9 is given in Fig. 2. The coordinates of GCPs were determined using continuously operating reference station networks (CORS) and a real-time kinematic global navigation satellite system (GNSS) using a virtual reference station. This procedure was carried out using a CHC X91 GNSS (CHC, Shanghai, China). The Yenice CORS station (35 km from the Etili site and 15 km from the Comakli site) was used as a reference point during our survey. The root-mean-square error of our measurements was less than 16 mm horizontally

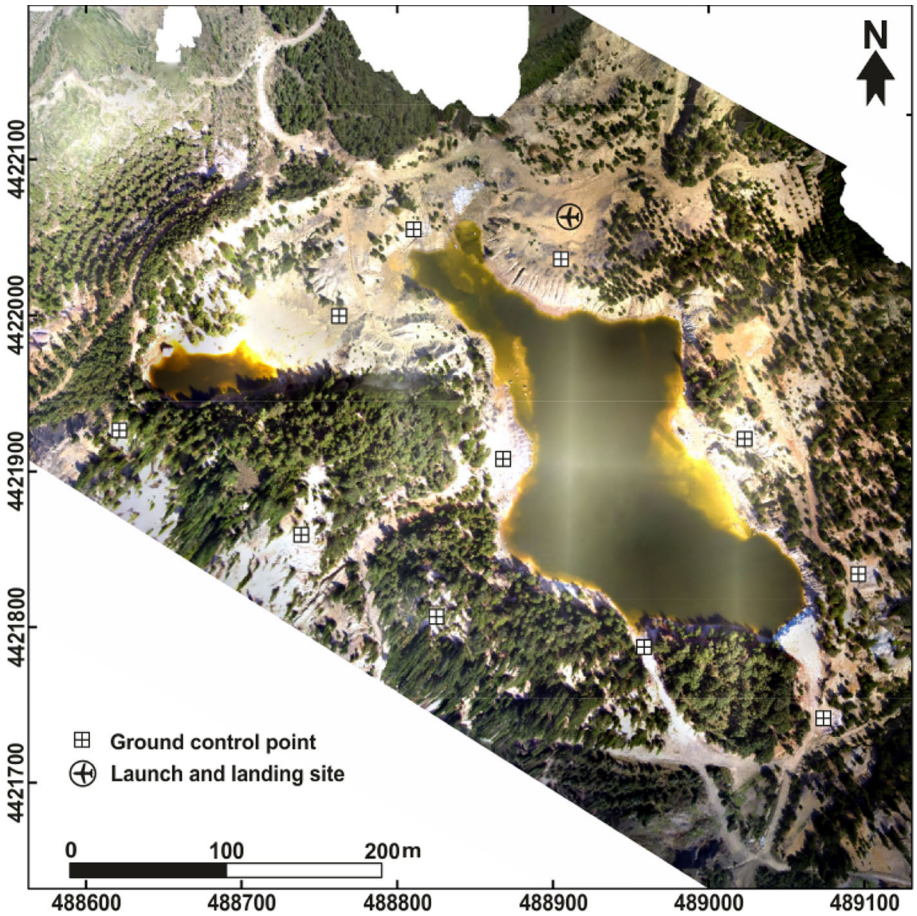

Fig. 2 Ground control point locations around E1 and E9

and 27 mm vertically. Horizontal coordinates were determined using the Universal Transverse Mercator (UTM) zone 35N (WGS84) projection, with vertical elevation determined using the mean sea level from the Turkey Hybrid Geoid 2009 (THG-09).

3.2 Unmanned Aerial Vehicle System Specifications

In this study, a DJI F550 model multirotor airframe hexacopter (Da-Jiang Innovations Science and Technology Co., Ltd., China) was used as the UAV (Fig. 3). It includes motors and propellers, an ArduPilot autopilot system, a global positioning system, a telemetry system, and a 16-channel 2.4 GHz radio controller. The settings for the autopilot control card, propeller, and radio controller of the UAV were calibrated, and the flight plan was set using its Mission Planner software. During the flights, 5000 mAh and three-cell LiPo batteries were used. The total weight of the UAV system is 2 kg, excluding the battery and camera. Battery weights vary from 200 to 450 g depending on cell size and capacity. The system flight time was 13 min for 5000 mAh batteries. The photographic capturing process was carried out at 30–100-m height, using a 12 megapixel (4000 × 3000 pixels) GoPro Hero3 digital camera (weighing 136 g with housing), which captured JPEG format images within the visible light range.

While preparing the flight plan, the "UAV home point" was selected as the takeoff point. In emergencies (strong wind, drift with turbulence, reduced battery), the UAV automatically landed at the home point, using coordinates determined from the GPS on the hexacopter. During the flight, waypoints, flight path, return points, and flight height were determined for each flight. To avoid negative weather conditions, and the hexacopter leaving the operator's sight range, flights were not more than 100 m above the ground. Geospatial details were at the same scale for images taken on flights at a fixed height, making image-matching procedures more precise.

3.3 3 Unmanned Aerial Vehicle Survey

During this study, images of mine lakes at both Etili and Comakli sites that had been previously identified on satellite images from May and August 2013 were taken with a UAV on two different occasions. However, ongoing mining activities at these sites led to the emptying of some mine lakes

Fig. 3 DJI F550 multirotor air frame hexacopter

Table 1 Overview of all UAV flights performed in November 2014

Flight	Lake name	Date	Start time (h:min)	Duration (min:s)	GCP	Area covered (ha)	Altitude (m, asl)	Flight altitude (m)	Resolution (cm/pxl)	Photos taken
1	E1	12 Nov 2014	15:02	05:14	11	31	245	60	3	315
	E9						230			
2	E8	12 Nov 2014	16:11	01:56	6	2	226	40	3	117
3	E6	12 Nov 2014	10:36	01:48	6	2	223	40	2	109
4	E7	12 Nov 2014	11:12	02:00	6	3	149	30	2	121
5	E2	12 Nov 2014	12:32	04:35	9	15	172	55	3	276
6	E4	16 Nov 2014	11:05	05:35	7	11	140	50	3	336
7	E5	16 Nov 2014	11:55	06:49	10	13	128	50	3	410
8	C1	16 Nov 2014	15:02	07:01	15	30	168	100	6	422
9	C2	16 Nov 2014	15:58	02:37	6	12	139	30	1	158
10	C3	16 Nov 2014	16:45	06:21	15	35	159	100	6	382
	C4						162			

during the study period. As a result, images could not be acquired for E3 in November 2014 and October 2015 and for C2 in October 2015. Stable flight of the UAV increased image quality and precision, while wind reduced it. To mitigate wind effects, flights were completed from 10:30 to 12:30 and from 15:00 to 16:30, when wind strength was lowest. The UAV was auto-launched from a flat area near each mine lake and was set to perform an auto-landing on these same flat areas. In spite of setting up a fixed flight path, manual control negatively affected image quality and resolution, especially in windy conditions. Thus, images were acquired at fixed height, under automatic flight control, while manual control was used for landings.

Before the flights, the lateral image overlap was calculated to be 60 %, with a longitudinal image overlap of 70 %, for a setting of one photograph per second. Each of the 10 flights in 2014 and nine flights in 2015 had its own fixed height for UAV image capture. Flight altitudes ranged from 30 to 100 m, depending on the size of the lake and height of surrounding trees. Because low-altitude flights boost image quality and resolution, when there was no geographical obstruction, image acquisition was performed at 30-m height. However, low-altitude flights over large lakes resulted in photographs encompassing wholly or predominantly lake surfaces. Image matching could not be performed on these photographs, as there were insufficient numbers of details to match on image pairs, leading to a reduction in orthomosaic resolution and the

Table 2 Overview of all UAV flights performed in October 2015

Flight	Lake name	Date	Start time (h:min)	Duration (min:s)	GCP	Area covered (ha)	Altitude (m, asl)	Flight altitude (m)	Resolution (cm/pxl)	Photos taken
1	E1 E9	10 Oct 2015	10:33	09:13	11	36	245 203	60	3	554
2	E8	10 Oct 2015	11:35	03:11	6	4	226	40	2	192
3	E6	10 Oct 2015	15:02	02:38	6	4	223	40	2	159
4	E7	10 Oct 2015	15:55	03:05	6	6	149	30	1	186
5	E2	17 Oct 2015	11:35	08:05	9	23	172	55	2	486
6	E4	17 Oct 2015	12:20	07:38	7	15	140	50	2	459
7	E5	17 Oct 2015	13:16	07:50	10	16	128	50	2	471
8	C1	17 Oct 2015	15:32	07:49	15	32	168	100	4	470
9	C3 C4	17 Oct 2015	16:23	08:03	15	43	159 162	100	5	484

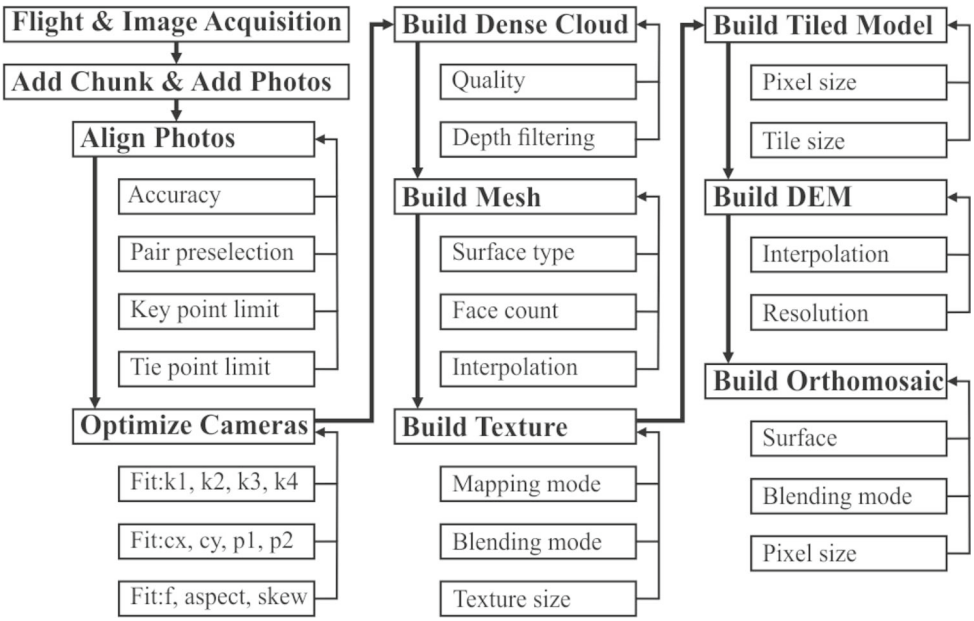

Fig. 4 Agisoft PhotoScan workflow steps

formation of spaces in orthomosaic and 3D surface models. Hence, for large lakes, images were collected from flights at 55–10-m height. Tables 1 and 2 include specifications of UAV flights. For example, the first flight was carried out over E1 and E9 lakes at an elevation of 245 m above mean sea level, at a flight height 60 m on October 10, 2015. This flight began at 10:13 am and lasted 9 min and 13 s. It used 11 GCPs, captured 552 photographs, and imaged a 36 ha terrain area. After image processing, an orthomosaic was created with resolution of 3 cm/pixel (see Table 2). Over the two consecutive years of this study, 19 mine lakes were imaged over a period of 4 days. All flights captured between 109 and 554 photographs, encompassing terrain areas from 2 to 43 ha. These images were used to generate orthomosaics, with resolutions of 1–6 cm/pixel, based on 6–15 GCPs, with flight durations from 1 min 48 s to 9 min 13 s.

4 Results and Discussion

4.1 Image Processing and 3D Modeling

Image processing used the workflow based on the SfM method in the Agisoft PhotoScan (version 1.2.0) software. This process created orthophotos and DEMs of mine lakes, mine waste, and natural topography. Images were matched using the functions: align photos and optimize cameras. Using camera position and orientation, a 3D point cloud (tie points) was created. Data from the 3D point cloud had depth filtering applied to create a 3D dense cloud. Using the 3D dense cloud points and the nearest neighborhood interpolation method, a 3D surface model (wireframe, solid, shaded, textured) and later a DEM and orthomosaic were created. The Agisoft workflow steps are shown in Fig. 4.

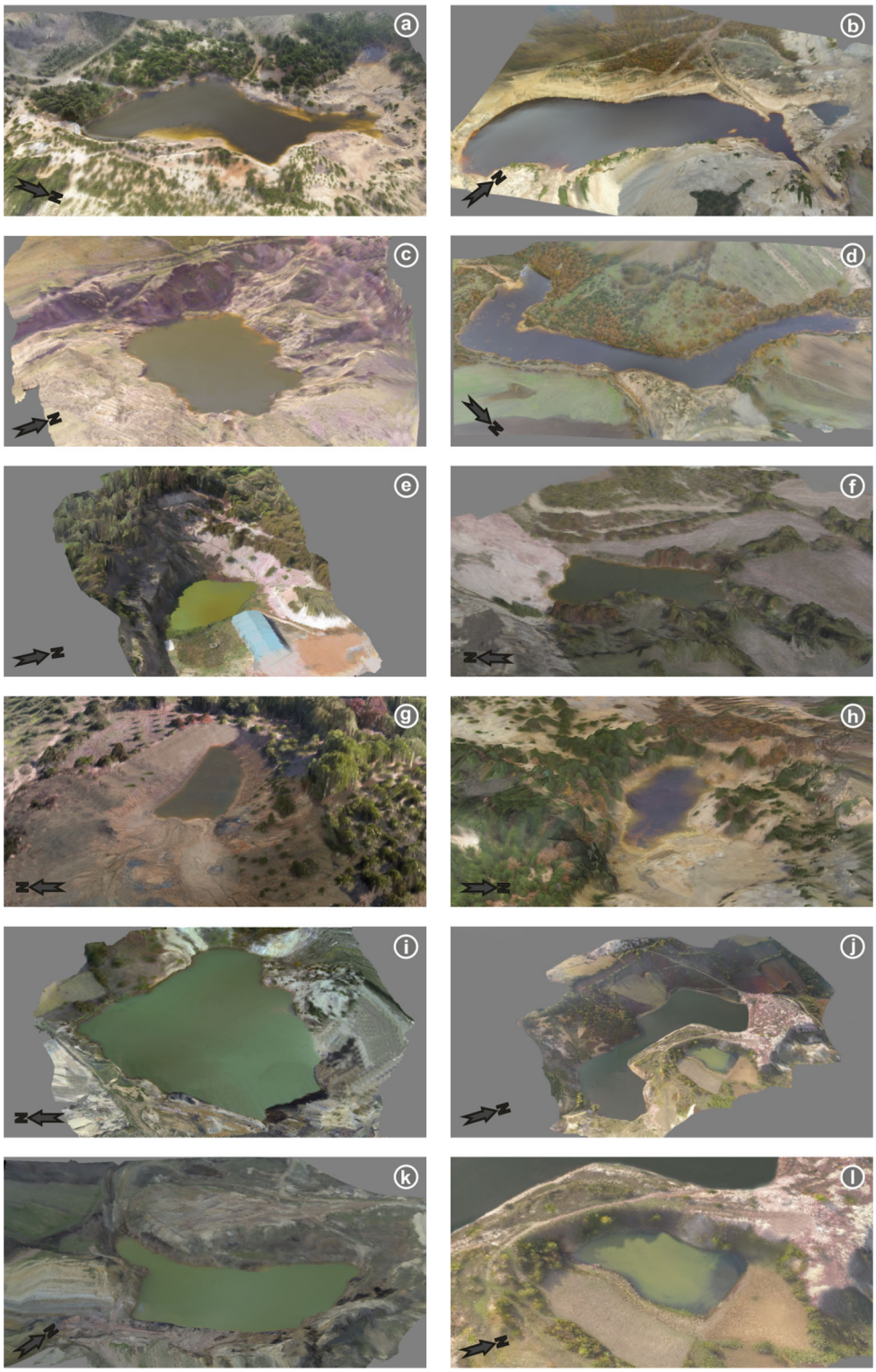

Fig. 5 3D terrain model of the mine lakes in November 2014. **a** E1, **b** E2, **c** E4, **d** E5, **e** E6, **f** E7, **g** E8, **h** E9, **i** C1, **j** C3, **k** C2, **l** C4,

Matching of images with few geospatial details can be resolved by placing additional GCPs, e.g., on lake surfaces. However, instead of this expensive and difficult procedure, flight heights were increased over large lakes to ensure that each image contained sufficient geospatial details, although high-altitude flights lower the resolution of the resulting orthomosaic. For example, images acquired at 30-m flight height had an orthomosaic resolution of 1 cm/pixel, while those acquired at 100-m flight height had their orthomosaic resolution reduced to 6 cm/pixel. In addition, shine and shad-

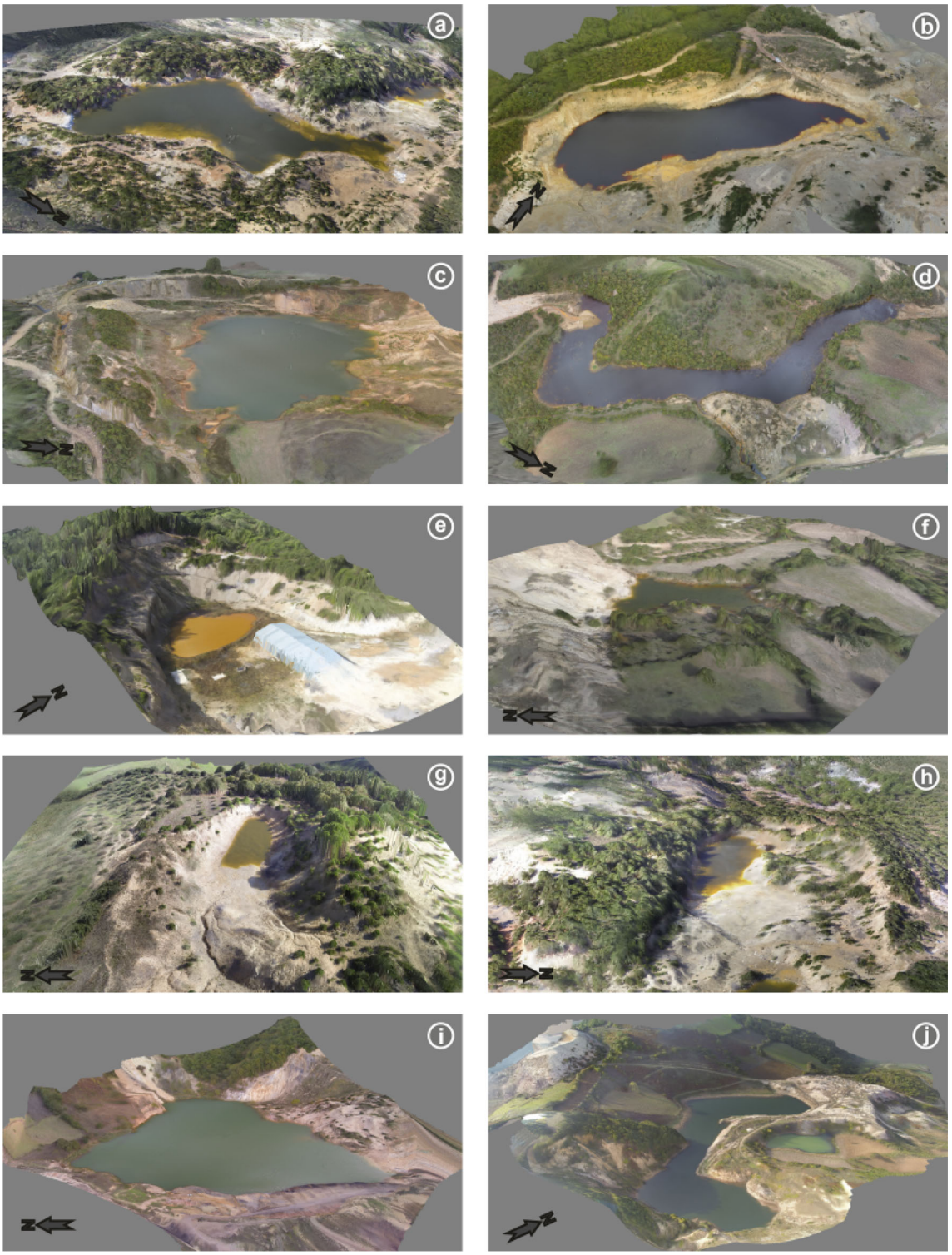

Fig. 6 3D terrain model of the mine lakes in October 2015. **a** E1, **b** E2, **c** E4, **d** E5, **e** E6, **f** E7, **g** E8, **h** E9, **i** C1, **j** C3 and C4

ows, detected as depth on the lake surface by the software, caused depressions and rises to be created on dense cloud and 3D surface models. This problem was resolved by creating a DEM after deleting erroneous points on the dense cloud, then using ArcHydro fill and sink tools (Esri, CA, USA) to generate the DEM. Using an accurate DEM and orthomosaic, 3D terrain models were created. The 3D terrain models created from images captured in November 2014 and October

Table 3 Area of mine lakes (from Worldview-1 and Pleiades satellite images, m^2)

Satellite	Date	Resolution	Etili site									Comakli site				Total
			E1	E2	E3	E4	E5	E6	E7	E8	E9	C1	C2	C3	C4	
Worldview-1[a]	3.15.2011	50 cm	31,654	20,768	14,407	25,543	23,830	611	2912	1441	3114	–	–	–	–	124,280
Pleiades	5.18.2013	50 cm	33,688	34,125	14,039	26,531	21,181	5596	2457	2039	5917	–	–	–	–	145,573
	8.4.2013	50 cm	–	–	–	–	–	–	–	–	–	84,494	16,539	57,494	7601	166,128

[a] This data provided by Sanliyuksel Yucel et al. [44]

2015 are presented in Figs. 5 and 6. Using these models, the morphologic and anthropogenic changes to the mine lakes could be precisely determined at high resolution. Furthermore, spatial surface analysis will be carried out using slope and aspect, based on DEM data in future studies.

4.2 Areal Change Detection

Using satellite images, it was determined that coal mining at the Etili site began at the beginning of the 1980s in the area near E1 [44]. Mining from 1985 to 1987 created E2 and E3, the first mine lakes at the Etili site. With no rehabilitation, abandoned coal mines formed lakes E1, E6, E8, E9, and E7 from 1987 to 1999, while E5 and E4 formed between 2003 and 2008. Using Worldview-1 satellite images from 2011, the total area of the Etili mine lakes was calculated to be 12.42 ha [44]. In May 2013, on Pleiades satellite images, the total area of mine lakes reached 14.55 ha (Table 3). The mine lakes at the Comakli site have not been previously studied using remote sensing methods. However, on Pleiades satellite images from August 2013, the total area of the mine lakes at the Comakli site was calculated to be 16.61 ha.

This study used high-resolution UAV images to determine lake borders based on two different methods in ArcGIS (version 10.3; Esri). Both a digitization method and a classification method of maximum likelihood classification (MLC) were used to extract lake boundaries. MLC is an effective standard classification method, having a generative model that assumes that the image features within each target class follow a Gaussian distribution [46,47]. This method determines sample areas on the lake to create as signature files.

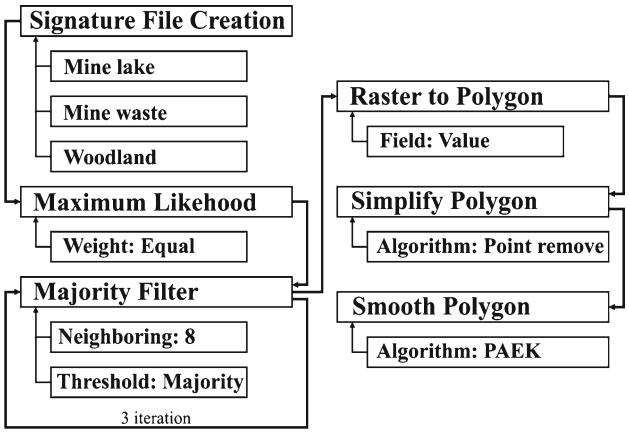

Fig. 7 Classification process steps on ArcGIS

Using the signature file, classified raster data of mine lakes are generated. A majority filter is performed three times on these classified data to generate image contrast. Later, a raster to polygon method is used to transform lake edges into vector data. The lake edges are generalized using simplify polygon and smooth polygon processing steps. This classification process is shown in Fig. 7. When areas for the mine lakes generated using both digitization and classification methods are compared, there appears to be a 1.1–4.8 % difference between the two methods (Table 4). This difference is related to differences in colors within and outside the lakes at each site. However, because black was selected as the contrast, the results of the two methods are similar. The result for E2 using the MLC classification method is given in Fig. 8a, while the borders determined using the digitization and classification methods are given in Fig. 8b. The classification method has

Table 4 Area of mine lakes (from UAV images, m^2)

Date	Method	E1	E2	E3	E4	E5	E6	E7	E8	E9	C1	C2	C3	C4	Total
12–16 Nov 2014	Digitizing	29,253	32,450	–	25,443	19,655	2327	2288	615	2287	80,054	16,129	42,815	5120	258,436
	Classification	28,072	32,098	–	24,625	18,950	2291	2234	600	2230	77939	15793	40,987	4947	250,766
	% Difference	4	1.1	–	3.2	3.6	1.5	2.4	2.4	2.5	2.6	2.1	4.3	3.4	–
10–17 Oct 2015	Digitizing	28,506	20,158	–	24,378	18,196	2168	2103	546	2154	72,789	–	41,392	4684	217,074
	Classification	27,319	19,916	–	23,669	17,608	2143	2045	535	2218	71,349	–	39,405	4500	210,707
	% Difference	4.2	1.2	–	2.9	3.2	1.2	2.8	2	3	2	–	4.8	3.9	–

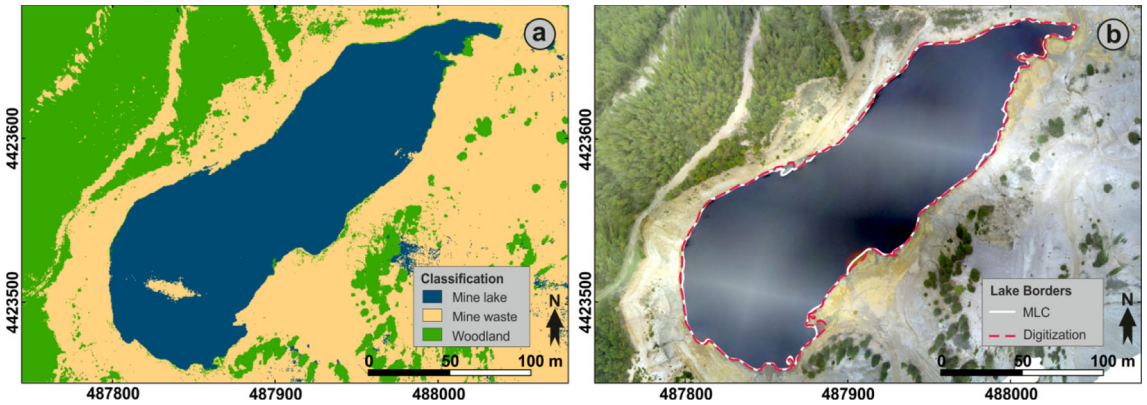

Fig. 8 **a** Classification map of E2 **b** Digitization and MLC method results

more errors in shallow sections of the lakes, where shadows fall on the lake, or the lake and area outside the lake have similar colors. Defining these areas while creating the signature file reduced this problem.

The UAV study of the Etili site in November 2014 gave the total area of the lakes as 11.42 ha. The reduction in area compared with satellite images from 2013 is related to the reopening of mining activities in 2014 and the subsequent emptying of E3. According to UAV data from 2015, the lake area was reduced to 9.82 ha, as E2 also was partially emptied. At the Comakli site, the total lake area was calculated to be 14.41 ha during UAV studies in November 2014. More recent field studies found that coal mining activity had recommenced in 2015, with C1 partially filled with waste, and C2 emptied. UAV images from October 2015 found that the lake area at the Comakli site had been reduced to 11.88 ha. Finally, the area of the lakes without anthropogenic intervention was larger in November 2014 than in October 2015. The reason for this is related to mean precipitation. Average monthly precipitation in October is 56.2 mm, but increases to 86.2 mm in November, according to the meteorological data covering 1950–2015 from the Canakkale Meteorological Station. Because the lakes are quickly affected by rainfall, meteorological factors also create short-term changes to lake morphology.

5 Conclusions

This study monitored mine lakes in 2014 and 2015 at the Etili and Comakli mine sites in the Can Coal Basin for the first time using low-cost, high-resolution UAV images. From UAV images, 3D point cloud, high-resolution orthomosaics, and 3D terrain models were created using the SfM method in the Agisoft software. While the resolution of satellite images obtained in 2013 was 50 cm/pixel, the resolution of images obtained by the UAV in this study was between 1 and 6 cm/pixel. As UAV images have higher resolution than satellite images, they provide more accurate spatial data. Additionally, there is no problem generating periodic data, in contrast to satellite images. The areas of mine lakes at the Etili and Comakli sites were determined using digitization and MLC methods. When the two methods were compared, the difference between the lake areas varied from 1.1 to 4.8 %. Such differences reflect the difference between the color of the lake and its surrounding area. While the total area of the mine lakes was 25.33 ha in November 2014, it was only 21.24 ha in October 2015. This areal reduction occurred because E2 and C1 were partially emptied, while C2 was fully emptied. Mine lakes with no anthropogenic intervention (E1, E4, E5, E6, E7, E8, E9, C3 and C4) showed changes related to meteorological factors. High-resolution UAV imaging is a rapid and appropriate method to determine morphologic properties and changes in mine lakes formed in open-pit coal mines, and to monitor their short-term anthropogenic and meteorological effects.

Acknowledgments The authors would like to thank Dr. Deniz Sanliyuksel Yucel for her insightful comments and Sahin May for his help during field studies. The authors are also thankful for constructive comments by the reviewers.

References

1. Eisenbeiss, H.: A mini Unmanned Aerial Vehicles (UAVs): system overview and image acquisition. In: International Archives of Photogrammetry, Remote Sensing and Spatial Information Sciences, International Workshop on Processing and Visualization Using High Resolution Imagery, vol. 36-5/W1, Pitsanulok, Thailand (2004)
2. Wang, Q.; Wu, Li.; Chen, S.; Shu, D.; Xu, Z.; Li, F.; Wang, R.: Accuracy evaluation of 3D geometry from low-attitude uav images: a case study at Zijin Mine. In: Proceedings of ISPRS Technical Commission IV Symposium, The International Archives of the Photogrammetry, Remote Sensing and Spatial Information Sciences, vol. XL/4, Suzhou, China, pp. 297–300 (2014)

3. Lucieer, A.; de Jong, S.M.; Turner, D.: Mapping landslide displacements using Structure from Motion (SfM) and image correlation of multi-temporal UAV photography. Prog. Phys. Geogr. **38**, 97–119 (2013)
4. Niethammer, U.; James, M.R.; Rothmund, S.; Travelletti, J.; Joswig, M.: UAV-based remote sensing of the Super-Sauze landslide: Evaluation and results. Eng. Geol. **12**, 2–11 (2012)
5. Ouédraogo, M.M.; Degré, A.; Debouche, C.; Lisein, J.: The evaluation of unmanned aerial system-based photogrammetry and terrestrial laser scanning to generate DEMs of agricultural watersheds. Geomorphology **214**, 339–355 (2014)
6. Mancini, F.; Dubbini, M.; Gattelli, M.; Stecchi, F.; Fabbri, S.; Gabbianelli, G.: Using unmanned aerial vehicles (UAV) for high resolution reconstruction of topography: The structure from motion approach on coastal environments. Remote Sens. **5**(12), 6880–6898 (2013)
7. Immerzeel, W.W.; Kraaijenbrink, P.D.A.; Shea, J.M.; Shrestha, A.B.; Pellicciotti, F.; Bierkens, M.F.P.; Jong, S.M.: High-resolution monitoring of Himalayan glacier dynamics using unmanned aerial vehicles. Remote Sens. Environ. **150**, 93–103 (2014)
8. Siebert, S.; Teizer, J.: Mobile 3D mapping for surveying earthwork projects using an Unmanned Aerial Vehicle (UAV) system. Autom. Constr. **41**, 1–14 (2014)
9. Martin, P.G.; Payton, O.D.; Fardoulis, J.S.; Richards, D.A.; Scott, T.B.: The use of unmanned aerial systems for the mapping of legacy uranium mines. J. Environ. Radioact. **143**, 135–140 (2015)
10. Douterloigne, K.; Gautama, S.; Philips, W.: On the accuracy of 3D landscapes from UAV image data. In: Proceedings of IGARSS 2010, Honolulu, Hawaii, USA. IEEE, pp. 589–592 (2010)
11. James, M.R.; Robson, S.: Straightforward reconstruction of 3D surfaces and topography with a camera: Accuracy and geoscience application. J. Geophys. Res. **117**, 1–23 (2012)
12. Fonstad, M.A.; Dietrich, J.T.; Courville, B.C.; Jensen, J.L.; Carbonneau, P.E.: Topographic structure from motion: A new development in photogrammetric measurement. Earth Surf. Proc. Land. **38**(4), 421–430 (2013)
13. Lowe, D.G.: Distinctive image features from scale-invariant keypoints. Int. J. Comput. Vis. **60**(2), 91–110 (2004)
14. Koutsoudis, A.; Vidmar, B.; Ioannakis, G.; Arnaoutoglou, F.: Performance evaluation of a multi-image 3D reconstruction software on a low-feature artifact. J. Archaeol. Sci. **40**, 4450–4456 (2013)
15. Javernick, L.; Brasington, J.; Caruso, B.: Modelling the topography of shallow braided rivers using Structure-from-Motion photogrammetry. Geomorphology **213**, 166–182 (2014)
16. Goncalves, J.A.; Henriques, R.: UAV photogrammetry for topographic monitoring of coastal areas. ISPRS J. Photogramm. **104**, 101–111 (2015)
17. Tavani, S.; Granadob, P.; Corradettia, A.; Girundoa, M.; Iannacea, A.; Arbuésb, P.; Muñozb, J.A.; Mazzolia, S.: Building a virtual outcrop, extracting geological information from it, and sharing the results in Google Earth via Open Plot and Photoscan: An example from the Khaviz Anticline (Iran). Comput. Geosci. **63**(2), 44–53 (2014)
18. Hirschmüller, H.: Accurate and efficient stereo processing by semi-global matching and mutual information. In: Proceedings of IEEE Conference for Computer Vision and Pattern Recognition, vol. 2, San Diego, CA, USA, pp. 807–814 (2005)
19. Ahmadabadiana, A.H.; Robson, S.; Boehm, J.; Shortis, M.; Wenzel, K.; Fritsch, D.: A comparison of dense matching algorithms for scaled surface reconstruction using stereo camera rigs. ISPRS J. Photogramm. **78**, 157–167 (2013)
20. Pierrot-Deseilligny, M.; Paparoditis, N.: A multire solution and optimization-based image matching approach: an application to surface reconstruction from SPOT5-HRS stereo imagery. Remote Sens. Spat. Inf. Sci. **36**(I1/W41), 73–77 (2006)
21. Furukawa, Y.; Ponce, J.: Accurate camera calibration from multi-view stereo and bundle adjustment. Int. J. Comput. Vis. **84**, 257–268 (2009)
22. Ducke, B.; Score, D.; Reeves, J.: Multiview 3D reconstruction of the archaeological site at Weymouth from image series. Comput. Graph. **35**, 375–382 (2010)
23. Nicosevici, T.; Garcia, R.: Efficient 3D Scene Modeling and Mosaicing. Springer, Berlin (2013)
24. Westoby, M.; Brasington, J.; Glasser, N.F.; Hambrey, M.J.; Reyonds, M.J.: Structure from motion photogrammetry: a low-cost, effective tool for geoscience applications. Geomorphology **179**, 300–314 (2012)
25. Foley, J.A.; DeFries, R.; Asner, G.P.; Barford, C.; Bonan, G.; Carpenter, S.R.; Chapin, F.S.; Coel, M.T.; Daily, G.C.; Gibbs, H.K.; Helkowski, J.H.; Holloway, T.; Howard, E.A.; Kucharik, C.J.; Monfreda, C.; Patz, J.A.; Prentice, I.C.; Ramankutty, N.; Snyder, P.K.: Global consequences of land use. Science **309**(5734), 570–574 (2005)
26. Tarolli, P.: High-resolution topography for understanding Earth surface processes: opportunities and challenges. Geomorphology **216**, 295–312 (2014)
27. Ellis, E.C.: Anthropogenic transformation of the terrestrial biosphere. Philos. Trans. R. Soc. A. **369**, 1010–1035 (2011)
28. Vanacker, V.; Bellin, N.; Molina, A.; Kubik, P.W.: Erosion regulation as a function of human disturbances to vegetation cover: a conceptual model. Landsc. Ecol. **29**, 293–309 (2014)
29. Chen, J.; Li, K.; Chang, K.; Sofia, G.; Tarolli, P.: Open-pit mining geomorphic feature characterization. Int. J. Appl. Earth Obs. **42**, 76–86 (2015)
30. Herrera, G.; Tomas, R.; Vicente, F.; Lopez-Sanchez, J.M.; Mallorqui, J.J.; Mulas, J.: Mapping ground movements in open pit mining areas using differential SAR interferometry. Int. J. Rock Mech. Min. **47**(7), 1114–1125 (2010)
31. Martin-Duque, J.F.; Sanz, M.A.; Bodoque, J.M.; Lucia, A.; Martin-Moreno, C.: Restoring earth surface processes through landform design: A 13-year monitoring of a geomorphic reclamation model for quarries on slopes. Earth Surf. Proc. Land. **35**, 531–548 (2010)
32. Grande, J.A.; Torre, M.L.; Ceron, J.C.; Beltran, R.; Gomez, T.: Overall hydrochemical characterization of the Iberian Pyrite Belt. Main acid mine drainage-generating sources (Huelva, SW Spain). J. Hydrol. **390**, 123–130 (2010)
33. Forstner, U.; Wittmann, G.T.W.: Metal Pollution in the Aquatic Environment. Springer, Berlin (1983)
34. Malmstrom, M.E.; Berglund, S.; Jarsjo, J.: Combined effects of spatially variable flow and mineralogy on the attenuation of acid mine drainage in groundwater. Appl. Geochem. **23**, 1419–1436 (2008)
35. Chen, C.J.; Jiang, W.T.: Influence of waterfall aeration and seasonal temperature variation on the iron and arsenic attenuation rates in an acid mine drainage system. Appl. Geochem. **27**, 1966–1978 (2012)
36. Anawar, H.M.: Impact of climate change on acid mine drainage generation and contaminant transport in water ecosystems of semi-arid and arid mining areas. Phys. Chem. Earth **58-60**, 13–21 (2013)
37. Sanliyuksel Yucel, D.; Balcı, N.; Baba, A.: Generation of acid mine lakes associated with abandoned coal mines in NW Turkey. Arch. Environ. Contam. Toxicol. **70**(4), 757–782 (2016)
38. Bozcu, M.; Akgun, F.; Gurdal, G.; Yesilyurt, S.K.; Karaca, O.: Sedimentologic, petrologic, geochemical and palinologic examination of Can Yenice Bayramic (Canakkale) lignite basin [in Turkish]. Final Report of The Scientific and Technological Research Council of Turkey (TUBITAK), Project No: CAYDAG-105Y114. Ankara, Turkey (2008)
39. Gurdal, G.; Bozcu, M.: Petrographic characteristic and depositional environment of miocene Can Coals, Canakkale–Turkey. Int. J. Coal Geol. **85**, 143–160 (2011)

40. Gunduz, O.; Baba, A.: Fate of acidic mining lakes in Can lignite district, Turkey. In: Proceedings of the XXXVI IAH Congress Integrating Groundwater Science and Human Well-Being. Toyama, Japan, pp. 1–7 (2008)
41. Okumusoglu, D.; Gunduz, O.: Hydrochemical status of an acidic mining lake in Can-Canakkale, Turkey. Water Environ. Res. **85**, 604–620 (2013)
42. Sanliyuksel Yucel, D.; Baba, A.: Geochemical characterization of acid mine lakes and their effect on the environment, NW of Turkey. Arch. Environ. Contam. Toxicol. **64**(3), 357–376 (2013)
43. Sanliyuksel Yucel, D.; Baba, A.: Effects of acid mine lakes on water resources in Biga Peninsula, Turkey. The Second International Conference on Water, Energy and the Environment, Kusadasi, Turkey, p.59 (2013)
44. Sanliyuksel Yucel, D.; Yucel, M.A.; Baba, A.: Change detection and visualization of acid mine lakes using time series satellite image data in Geographic Information Systems (GIS): Can (Canakkale) County, NW Turkey. Environ. Earth Sci. **72**(11), 4311–4323 (2014)
45. Sanliyuksel D.; Baba A.: Effects of the abandoned mining wastes on water resources in Can Basin. In: 64th Geological Congress of Turkey, Ankara, pp.47–48 (2011)
46. Tokarczyk, P.; Leitao, J.P.; Rieckermann, J.; Schindler, K.; Blumensaat, F.: High-quality observation of surface imperviousness for urban runoff modeling using UAV imagery. Hydrol. Earth Syst. Sci. **12**, 1205–1245 (2015)
47. Ustuner, M.; Balik Sanli, F.; Dixon, B.: Application of support vector machines for land use classification using high-resolution rapid eye images: a sensitivity analysis. Eur. J. Remote Sens. **48**, 403–422 (2015)